PCCP

ROYAL SOCIETY OF CHEMISTRY

www.rsc.org/pccp

Large-scale synthesis and formation mechanism study of basic aluminium sulfate microcubic crystals

Yuguo Xia, Bo Chen, Xiuling Jiao,[*] and Dairong Chen

School of Chemistry & Chemical Engineering, National Engineering Research Center for colloidal materials,

Shandong University, Jinan 250100, P. R. China

Cubic-like basic aluminium sulfate crystals were prepared by a facile template-free hydrothermal strategy. The microstructures, morphologies and textual properties of as-synthesized material were characterized by X-ray diffraction (XRD), field-emission scanning electron microscopy (FE-SEM) and transmission electron microscopy. X-ray crystallography reveals cubic basic aluminium sulfate possesses single crystal nature. Chemical formation mechanism studies of sulfuric acid with γ-AlOOH were performed using a combined experimental and computational approach. Time dependent experiments reveal formation of basic aluminium sulfate is based on dissolution-recrystallization process, and source of Al^{3+} is only dissolved from γ-AlOOH in high H^+ concentration. Moreover, the quantum mechanical calculation reveals that dramatic structural changes occurred in (100) plane under high H^+ concentration which is inferred to be the initiation for source of Al^{3+}. Meanwhile, surface energy calculations can well explain the exposed plane of basic aluminium sulfate microcubes which is consistent with the XRD result. Besides, equations to quantitative describe the relationship of the molar amount of H^+ and final phase is proposed which has been confirmed by experimental results.

---

[*] Corresponding author, E-mail address: jiaoxl@sdu.edu.cn

Introduction

The chemical and physical properties of inorganic micro-/nanostructures are fundamentally related to their chemical composition, size, crystal structures and morphology. Getting control of these factors precisely is beneficial not only to observe unique properties of prepared materials but also to tune their chemical and physical properties as desired.[1] As a facile method, solution route exhibits advantages in tuning morphology and size of micro/nanocrystal simply by adjusting the solvent, temperature, additive, concentration, and etc. In previous reports, solution route has been successfully applied in preparing a series of micro/nanocrystals including metal, oxide and sulfide crystals with controlled morphology and size. However, limited by the rapid nucleation and crystal growth, this method has not been widely used in preparing insoluble inorganic salts.

Hydrated basic aluminum sulfate, a basic salt of aluminium, can be used as precursor for preparing various aluminas, catalysts and quality ceramic products.[2] However, limited by obtaining regular morphologies and getting knowledge of corresponding crystal structures and formation mechanism, basic aluminium sulfate still has not been widely used and studied even though its XRD pattern was detected since 1960s.[3] Many studies have been done to fabricate basic aluminium sulfate and study corresponding structures. In experiment, basic aluminium sulfate is mainly fabricated by precipitation[4] or sol-gel method.[5] However, well-defined basic aluminium sulfate particles is still not obtained mainly due to the coagulation or aggregation process during preparation derived from the rapid nucleation and crystal growth. In structure, basic aluminium sulfate possesses so-called Keggin-type $A1_{13}$ cage structure which is considered to be the basic building blocks for formation large aluminium hydroxide complex.[6] Nevertheless, even molecular formula of basic aluminium sulfate is in controversy because of the difference in fabricating materials. In present work, a facile hydrothermal approach was adopted to fabricate uniform-sized basic aluminum sulfate crystals with micrometer dimension. During the formation process of basic aluminum sulfate, the concentration of H^+ is considered to be the crucial factor, which can change the composition of final products and influence the dissolution process of Al^{3+}.[7] Moreover, it is found the formation process of basic aluminum sulfate undergoes dissolution–recrystallization mechanism and mono-disperse microcubes can be obtained only when the molar amount of H^+ is just sufficient for AlOOH dissolution. Besides, similar process has been found in α-FeOOH/H^+ system.[8] Thus, investigating the interaction of γ-AlOOH surfaces with H^+ is beneficial for controlling synthesis and understanding corresponding formation mechanism. Many experimental works have been done to characterize the boehmite/water interface with respect to acid/base properties.[9] However, most of the results are qualitative explanations based on experimental facts, which is not sufficiently accurate to understand the formation mechanism.

As supplementary means to experiments, quantum mechanical study is extremely useful approach to study reaction mechanism at atomic or molecular scale.[10] In the last fifteen years, many studies which are relevant to surface and morphology of γ-AlOOH have been performed with the aim to determine the most stable morphology in vacuum and water,[11] the relaxation and reconstruction of γ-AlOOH surfaces,[12] the dehydration process[13] and transfer process of H atoms on the boehmite/water interface.[14] However, all the calculations are based on the water environment without considering pH changes. Water is considered to plays little role in the interaction between cation/ anion and interface,[15] and H^+ is more preferential to interact with surface exposed O atoms than that in water considering the quantity of positive charge in H atom. Recently, we reported the interactions sulfate ions on the γ-AlOOH surfaces which mainly involved the adsorption process, and (010) and

(001) planes can be stabilized by surface protonation while (100) plane without surface hydroxyls is relative unstable and surface reconstruction may occurred under the effect of water or ions.[16] In present work, we mainly considered the surface structural changes of γ-AlOOH surfaces in acidic environment, and to our best knowledge, the interaction between (100) plane of γ-AlOOH and H^+ is studied for the first time.

Herein, the focus of present work is two-fold. First, we prepare the uniform single hydrated basic aluminum sulfate microcubes through a facile hydrothermal route, and give its crystal structure based on single crystal XRD analysis. Time dependent experiments are employed to study formation mechanism of basic aluminum sulfate. Second, calculations based on first principles density function theory are implemented to reveal the interaction of $AlOOH/H^+$ in different H^+ concentrations, which are analyzed in term of Mulliken charge population analysis and bond population. At the same time, morphology of basic aluminum sulfate is predicted based on the surface energy calculations to give an intuitive image. Experimental and computational results are combined to allow an understanding of formation mechanism of basic aluminum sulfate.

Experimental

Sample Preparation

All reagents in this study were used as received without further purification. In a typical synthesis, 18.0 g AlOOH raw nanoparticles (0.1 mol from Shandong Aluminum Corp.; its XRD pattern and TEM image are shown in Figure S1) were added into deionized water to form 100 mL well-dispersed suspension under vigorous stirring for 0.5 h, and 80 mmol H_2SO_4 was then added into this suspension. Treated by a quick stirring for 10 min and loaded in 25 mL autoclave with Teflon liner, the autoclave was heated at 240 °C for 2 h. After the autoclave was cooled to room temperature naturally, the white precipitate was collected by centrifugation at 8000 rmp for 10 min, washed with deionized water for three times, and then dried at 100 °C for 2 h. Additional experiments, as those above, but with changes of molar amount of H_2SO_4 to investigate the influence of H^+ to the final phase, were carried out too.

Characterization

Structures of the samples were identified by powder X-ray diffraction patterns obtained on a Rigaku D/Max 2200-PC diffractometer with the tube electric voltage and current of 40 kV and 35 mA for CuKα radiation (λ=0.15418 nm) at a scan rate of 2^o/min and scan step 0.02^o . Morphological analysis was performed by a field emission scanning electron microscope (FE-SEM, ZEISS SUPRATM 55) with an accelerating voltage of 5 kV and transmission electron microscopy (TEM JEM-100CXII) with an accelerating voltage of 80 kV. Single crystals X-ray diffraction measurement was collected with a Bruker Smart CCD area detector using a graphite monochromator and MoKα radiation (λ=0.71073 nm) at room temperature. Crystal structure was solved by using the program SHELXL and Fourier difference techniques, and refined by full-matrix least-squares method on F^2 data. All hydrogen atoms were added theoretically and details concerning the data collection and structure refinement are given in Table S1.

Electronic structure calculations

Structurally, γ-AlOOH has a lamellar structure within an orthorhombic symmetry. Each layer constitutes the (OAlOH-HOAlO) stacking sequence in the x- and y-direction as shown Figure S2. Here in this paper, γ-AlOOH single cell was derived from the experimental structure determined by Corbato et al, [17] and positions of the hydrogen atoms taken from the work of Hill et al.[18] All calculations in the present study were performed using the CASTEP program package.[19] The exchange-correlation functional was described by a generalized gradient approximation (GGA) [20] with the Perdew-Burke-Ernzerhof (PBE) scheme.[21] Interaction between the valence electrons and ion core was substituted by ultrasoft pseudopotentials which represented $1s^1$, $2s^2 2p^4$ and $3s^2 3p^1$ for H, O and Al atoms, respectively. The bulk boehmite with a size of 2.90 × 12.34 × 3.74 $Å^3$ was applied which had been optimized as shown in our previous work.[22] For all geometry optimizations and single energy calculations, self-consistent convergence accuracy was set at 1×10^{-5} eV/atom, the convergence criterion for the force between atoms was 3×10^{-2} eV/Å, and the maximum displacement was 1×10^{-3} Å.

On the basis of above set, the crystal was cleaved along (100) Miller planes to create γ-AlOOH slab. To simulate the reactions occurring on (100) plane in contact with H^+, (1×4) surface was modeled by periodically replicated slabs to construct the adsorption elemental slab which comprised 5 atoms layers with a 15 Å vacuum space normal to the layer. Additionally, top three atom layers of constructed slabs were unconstrained while the unsaturated atoms in the bottoms were coordinated with hydrogen atoms to eliminate the polarization effect. For all the adsorption structures, the geometrical optimization was implemented at the Γ point while 2×2×1 k-mesh was used for electronic property calculations based on the corresponding optimized geometries. DFT calculations were performed to observe the stable geometries and adsorption energies according to the equation followed.

$$E_{ads} = (E_{slab+adH^+} - E_{slab}) / \chi$$

Here, $E_{slab+adH^+}$ is the total energy of (100) slab and adsorbed H^+ after optimization, E_{slab} is the total energy of (100) slab and χ is the number of H^+. Energy of adsorbed H^+ is ignored.

Results and Discussion

Structure and morphology characterization of as-synthesized BAS microcubes

Figure 1 shows the typical XRD pattern of the hydrothermal sample and all the diffraction peaks can be readily indexed to basic aluminium sulfate (hereafter, BAS for short) with lattice constants *a*=7.018, *b*=7.018, and *c*=17.093 Å (space group: *R3m*, JCPDS: 16-0409). The strong intensity as directed by the arrow relative to that in standard card indicates the particles oriented perpendicular to (012) plane.

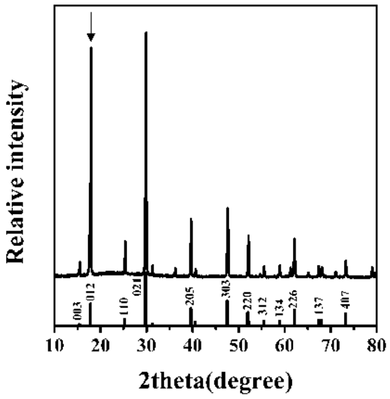

Figure 1. XRD patterns of the hydrothermal sample and that in JCPDS file.

X-ray crystallographic analysis is conducted to study the crystal structure, which reveals that BAS is a three-dimensional framework and crystallizes in trigonal *R3* space group, and the crystallographic details are summarized in Table S1. As shown in Figure 2a, there are three kinds of O atoms, O_1 linked with S atoms, O_2 in hydroxyl and O_3 existed in coordinated water. All the six coordinated aluminum atoms adopt [AlO_6] octahedron geometry, where four O atoms are O_1 and two are O_2. In nature, BAS has a lamellar structure and each layer constitutes the (SOAl-O-AlOS) stacking sequence in the a- and b-direction. The cohesion of the stacked layers in the c-direction is ensured by hydrogen bonds between hydroxyl groups belonging to two neighboring layers and forming a zig-zag chain along the c-direction. The XRD pattern simulated in Bragg-Brentano method without any further refinement is shown in Figure 2b. Most of peak positions and relative intensities are in good agreement with the data in standard card except those marked by the arrows which are also found in Figure 1. Noteworthy, the strongest peak around 30 ° should be ascribed to (113) plane which was wrongly labeled as (021) in JCPDS file, because the 2 theta difference between (113) and (021) is less than 0.01 °, which is hard to be detected by experimental instrument.

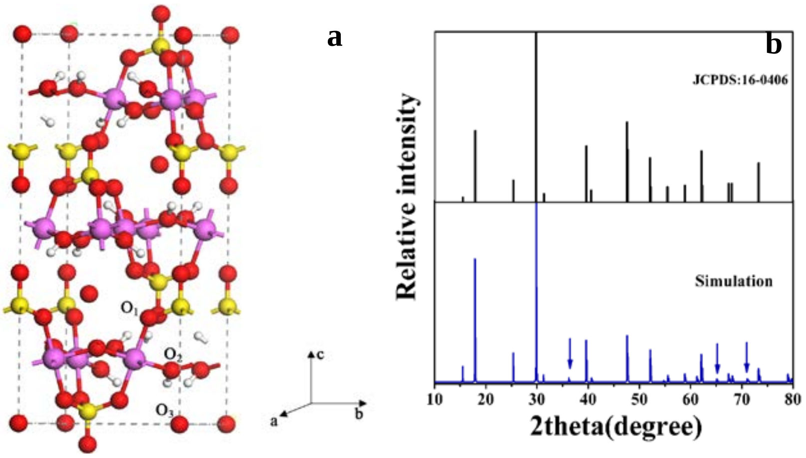

Figure 2. (a) Coordination environment of Al atom in BAS. Hydrogen atoms belonging to the coordinated water are omitted for clarity. Red, pink, white and yellow spheres represent aluminum, oxygen, hydrogen and sulfur atoms, respectively. (b) XRD pattern simulated from BAS single cell compared to standard card.

The morphology and microstructure of the as-prepared sample was further investigated by SEM as shown in Figure 3. The low-magnification SEM image (Figure 3a) shows that the product with regular morphology is composed of microcubes with size of 15.7±0.8 μm which indicates the good dispersity. Microstructures of other morphologies, such as irregular aggregations, were not observed, indicating a very high yield of the cubic-like crystals. The smooth surface as shown in high-magnification SEM image (Figure 3b) reveals the well-defined microcrystals have been formed which is consistent with our single crystal diffraction result. It is considered that formation of BAS may undergo the traditional crystal growth process proposed by Lamer and Dinegar.[23] Detailed discussion for the formation of BAS will be given in the following section. Moreover, the nearly monodisperse size illustrates second nucleation has been avoided during the hydrothermal treatment.

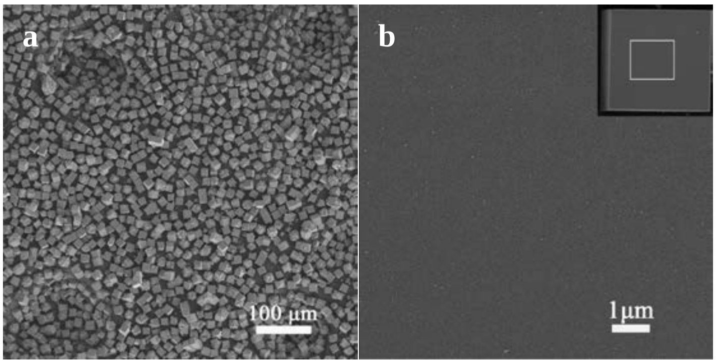

Figure 3. SEM images of the typical BAS particles, overall view (a) and surface structure (b).

Structural reconstruction of (100) plane under the effect of H^+ and BAS morphology predication

Usually, high index planes with unsaturated bonds are known as unstable ones which could transform into low index ones through surface reconstruction. It is found that the impact of H^+ in solution mainly reflected on the existence form of surface hydroxyls which is $R{\equiv}AlOH_2^+$ in $AlOOH/H^+$ system.[24] According to our previous work,[16] final morphology of AlOOH in sulfate acid system is decided by the competition of three growth directions [100], [010] and [001] as illustrated in the HRTEM images of Figure S3. Thus, it is rational to study the influence of H^+ to the final morphology through only calculating the interactions of H^+ with (100), (010) and (001) planes. While (010) and (001) planes of γ-AlOOH which are truncated with surface hydroxyls are considered to be stable after protonation, that is, (010) and (001) planes could be stabilized after protonation, surface reconstruction may take place on (100) plane without surface hydroxyls which has been proved by adsorption energy calculation. Thus, (100) is the most probable plane for source of Al^{3+} through dissolution under the effect of H^+.

On the basis of above analysis, interaction site for H^+ adsorbing on (100) plane was considered to be O atoms and three adsorption structures representing different H^+ concentration were constructed: (a) single H^+ adsorption model to simulate the relative low concentration of H^+ which was just sufficient for surface hydroxyls protonation, (b) double H^+ adsorbing on independent O atoms model to simulate the moderate concentration of H^+ which could cause protonation for (100) plane without hydroxyls, and (c) double H^+ adsorbing on the same O atom model to simulate the relative high concentration of H^+ which may induced the dissolution of AlOOH to Al^{3+}. The initiative three adsorption structures and corresponding geometric structures after optimization are shown in Figure 4. For the sake of comparing the differences in three conditions, bond lengths, Mulliken charge, bond populations and adsorption energy were calculated as shown in Table 1.

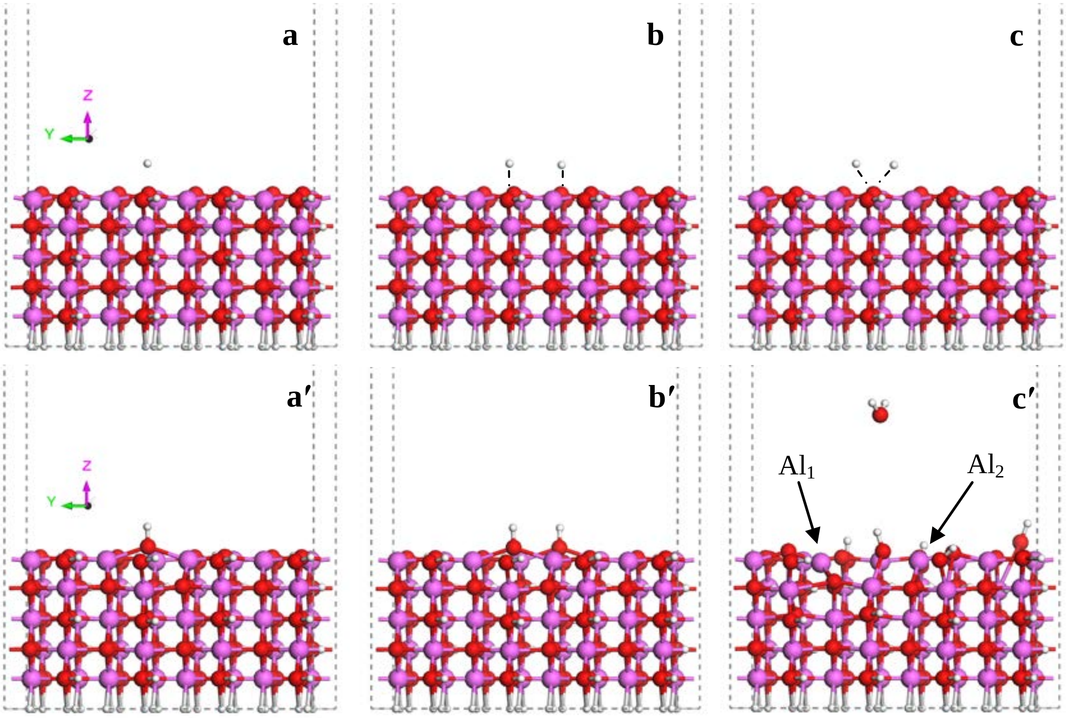

Figure 4. Three adsorption structures of H^+ on (100) plane of γ-AlOOH, initial structures (a), (b) and (c) and corresponding structures after optimization (a′), (b′) and (c′).

The coordination number can, depending on the exposed plane, be involved in protonation, deprotonation and complexation reactions with metal ions and ligands.[25] One important parameter to determine, when studying surface properties and modeling the metal oxide/inorganic ion, is the Al surface coordination number which is considered to be related to the surface reactivity of Al oxides and hydroxides. Summarizing the adsorption energies listed in Table 1, it is found that, for single H^+ adsorption in model a, the E_{ads} is positive, indicating that (100) plane of AlOOH decorated by single H^+ is unstable and surface reconstruction may occur which is in accordance with our former result. To the contrary, E_{ads} in model b and c are all negative, which illustrates it is beneficial for H^+ absorbing on (100) plane in relative high H^+ concentration. This conclusion raises two concerns that at first may have seemed contradictory. First, the surface reconstruction induced by H^+ adsorption causes the increase of total energy. Second, the formation of O-H bonds lowers the surface polarization of (100) plane, because all the O atoms in bulk are 4 coordinated while it is 3 coordinated on the surface. Obviously, the formation of O-H bond is more beneficial to the structural stability, and it is proved that (100) plane under fully surface protonation state is the most stable structure as shown in Figure S4. Noteworthily, unlike the nearly unchanged surface structures in model a and b, structural reconstruction occurs in model c especially for the coordination number of Al as directed by the arrow changing from Al_{IV} to Al_{III} due to the removal of water, which is inferred to be the initiation for the dissolution of AlOOH.

To understand the charge redistribution induced by H^+, Mulliken charge population was calculated, and bond population was used to evaluate the chemical bond type. Confessedly, the absolute values of atomic charges from the population analysis have little physical meaning, but useful information can be drawn from the relative values of Mulliken population. As shown in Table 1, charge, bond length and bond population changed little, indicating that surface protonation process in model a and b was relative independent among adjacent O atoms. However, the length of Al-O bond in model c (Al_1-O, 1.673 Å and Al_2-O, 1.741 Å) is shortened relative to that in unprotonated surface (1.891 Å), which is considered to be caused by the change of coordination number.

Table 1. Adsorption energies and electronic properties of H^+ adsorption on AlOOH (100) plane.

Model	Atom	Charge	Bond	Length/Å	Population	E_{ads}/eV
a	O	-1.01	O-H	0.995	0.54	12.31
	Al	1.90/1.90	Al-O	2.096/2.069	0.32/0.33	
b	O	-1.01	O-H	0.996	0.54	-12.27
	Al	1.91/1.91	Al-O	2.109/2.044	0.31/0.34	
c	O	-0.57	O-H	1.003	0.43	-14.77
	Al	1.92/1.93	Al-O	1.673/1.741	0.61/0.50	

To further explore the surface reconstruction of γ-AlOOH (100) plane under high H^+ concentration, on the basis of model c, structure with two H^+ put upon the same O atom which linked with Al_2 atom was constructed. As shown in Figure 5b, coordination number of Al_1 and Al_2 atoms recovered into 4-fold by sharing hydroxyl (μ_1-O-H), but dramatic structural changes occurred on Al_2 atom after optimization which deviates from original lattice plane. Herein, O atoms as labeled were considered to be more probable for H^+ attacking because of more negative charge (μ_1-O,-1.13*e* μ_2-O,-1.18*e*) relative to others (-1.07*e*) linked with Al_2 atom or surface protonated O atoms (-1.05*e* Figure S4). Consequently, μ_1-O-Al_1 and μ_2-O-Al bonds are lengthened after H^+ attacking at μ_1-O and μ_2-O atoms, resulting in the break of μ_1-O-Al_1 and μ_2-O-Al bonds and departure of $Al^{3+}$from (100) plane of γ-AlOOH in the form of $Al(H_2O)_4^{3+}$. Moreover, Al^{3+} is considered to be exists as an octahedral hexahydrate ion (6-fold coordinated) in acidic solutions [26] while static DFT calculation reveals Al^{3+} preferred to be 5-fold coordinated.[27] Herein, we only focus on the surface reconstruction of γ-AlOOH (100) plane under the effect of H^+, and the stable existed form of Al^{3+} monomer along with corresponding oligomerization mechanism in sulfuric acid needs to be further investigated.

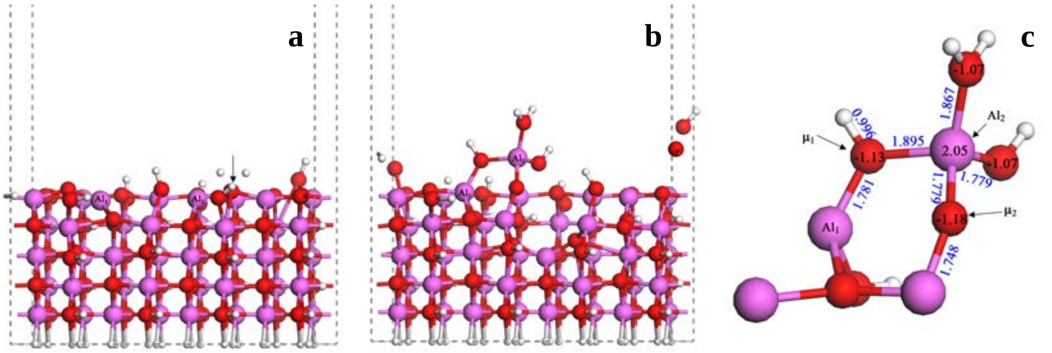

Figure 5. Adsorption structure of H^+ on (100) plane of γ-AlOOH: initial structure (a), structure after optimization (b) and corresponding structural parameters (c). Charges are in black font and bond lengths are in blue font.

The relationship between the crystal morphology and the internal arrangement of atoms in the crystal is therefore of great interest to chemists, chemical engineers and process engineers. Rationalization of this relationship allows the prediction of crystal shape, the development of tailor-made additives, and the control of solvent and impurity effects.[28] Usually, crystals with specific morphology are usually obtained by its intrinsic properties or adding morphology decorated reagents.[29] According to the classic Gibbs-Curie-Wulff law, the equilibrium crystal shape can be obtained by minimizing the total surface free energy for a fix volume, in which the length of a vector drawn normal to a crystal face (*hkl*) will be proportional to its surface energy γ_{hkl}. Herein, Bravais-Friedel Donnary-Harker (BFDH) method, which uses the crystal lattice and symmetry to generate a list of possible growth faces and relative growth rates, was adopted to qualitatively predict the most possible exposed planes and stable morphology. Figure 6a shows the possible exposed planes and morphology predicted and only three families of crystal planes, {012}, {101} and {003} were shown as the most possible exposed planes. As shown in Figure 6a, only {012} family of BAS crystal planes is square which is possible to form cubic-like BAS from geometrical configuration. Moreover, Combining XRD analysis aforementioned in which peak intensity of (012) obviously enhanced, it is considered that the exposed plane of as-prepared microcubes is {012}.

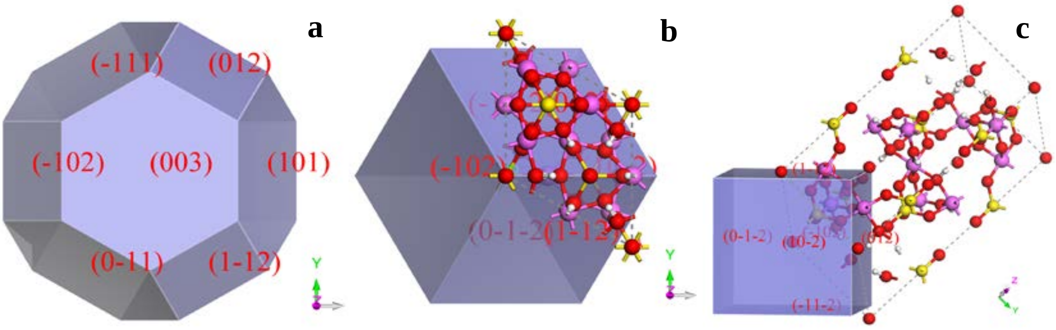

Figure 6. Possible morphologies predicted by BFDH method from trigonal single cell. (a) polyhedron with exposed planes of {003}, {101} and {012}, (b) (c) cube with exposed planes of {012}. (b) (view along C axis) and (c) (front view).

To verify above envisage and precisely determinate which is the exposed plane in as-prepared cubic microcrystal, standard method for calculating the surface energy is used to evaluate the total energy of a slab including N multiple single cell atoms and to subtract from the bulk energy obtained from a separate calculation according to the following equation.

$$\gamma = \lim_{n\to\infty}\frac{1}{2A}[E_{slab} - NE_{bulk}]$$

Here, E_{bulk}, E_{slab} and A represent the energy of bulk BAS, total energy of the bare slab after optimization and surface area, respectively.

In order to obtain the surface energies of (003), (101) and (012) planes, surpercells with only central one atom layer constrained structure were constructed, corresponding to periodically bounded surfaces, and the length of boxes was increased by 15 Å for both sides as extra vacuum space between the periodic images of the supercells as shown in Figure 7. Detailed parameters used for calculations and the surface energies of aforementioned exposed planes are listed in the Table S2. As shown in the calculated surface energies, (012) plane is the most stable plane with a surface energy of 860.4 mJ/m^2 while the surface energies for (101) and (003) planes are 1767.2 mJ/m^2 and 1622.8 mJ/m^2, respectively. Based on the result, the total energy of a BAS cube with exposed plane of {012} is much lower than that of a polyhedron with the exposed planes of {003}, {101} and {012} (Table S2), which illustrates cubic-like BAS exposing {012} planes is relative stable in our preparation condition.

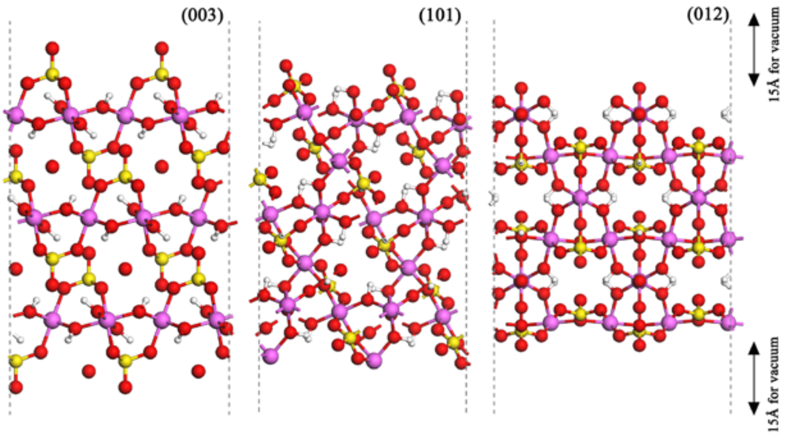

Figure 7. Structures for surface energy calculation, (a) (003) plane, (b) (101) plane, (c) (012) plane.

Formation mechanism for basic aluminium sulfate microcubes

It is well known that the formation of smaller crystallites is kinetically favored during the initial reaction stage while larger crystallites are thermodynamically favored. Getting knowledge of the formation mechanism of BAS is of great importance to obtain crystals with desired morphology and size.

To elucidate the formation process of BAS microcubes, time-dependent experiments were carried out. Figure 8 shows the morphology changes of the sample over time and corresponding phase changes are given out in Figure S5. Low-crystallized γ-AlOOH without definite morphology first appeared at the initial stage of hydrothermal reaction up to 30 min. With increasing time to 45 min, some irregular aggregates formed which was identified as weak-crystallized boehmite, because the relative peaks intensity belonging to boehmite phase increased. After 60 min, a great deal of nanoparticles with size of ca.6.0 nm was formed, which were considered to be the nuclei of BAS from XRD pattern. Prolonging hydrothermal time to 75 min resulted in BAS crystal, which was gradually developed into cubic-like morphology with ca.6.0 μm as shown in Figure 8d. Further prolonging hydrothermal time to 90 min, BAS as the major crystalline phase was detected and the microcubes grow up to ca.16 μm as shown in Figure 8e. Herein, hydrothermal time increased to 120 min is considered to be a process to completely deplete the AlOOH raw material and promote crystallization.

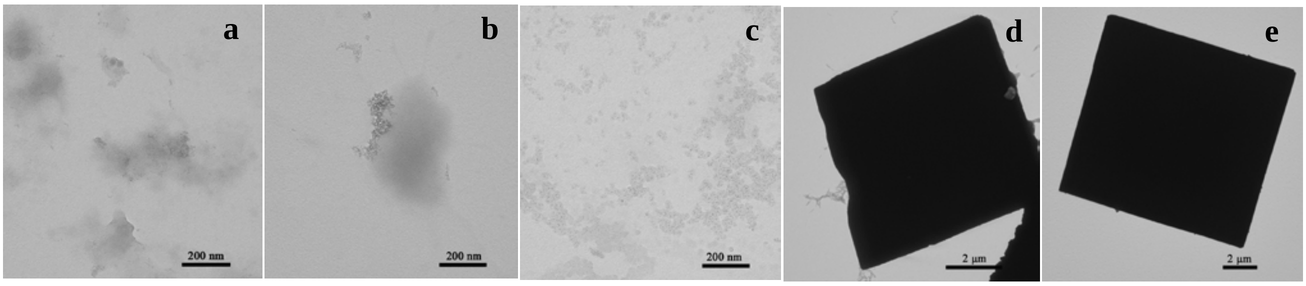

Figure 8. TEM images of time-depended experiments at 240 °C for different time: 30 min (a), 45 min (b), 60 min (c), 75 min (d), and 90 min (e).

Principally, the crystal formation is based on traditional growth and aggregation-induced growth mechanism. The obvious characteristic of aggregation-induced growth process is the coexistence of products and aggregation clusters during the formation process. Then, the intermediate at 75 min was investigated in detail, which was the mixture of BAS with smooth surface and γ-AlOOH nanorods, and no clusters were found (Figure S6). Therefore, it is considered that the formation of BAS cube should undergo the nucleation and traditional growth mechanism. Based on the above experimental results, the formation of BAS accompanied by dissolution of γ-AlOOH raw material to Al^{3+} is proposed. The dissolution of γ-AlOOH is the prerequisite for the formation of BAS microcubes, which can be described as follows:

$$\gamma\text{-}AlOOH + 3H^{+} \square \quad Al^{3+} + 2H_2O \qquad (1)$$

$$3Al^{3+} + 2SO_4^{2-} + 7H_2O \square \quad H_3OAl_3(SO_4)_2(OH)_6 + 5H^{+} (2)$$

Where equation (1) represents the dissolution process of γ-AlOOH and equation (2) represents the recrystallization process.

According to the DFT calculation, AlOOH dissolution process in equation (1) was speculated to initiate from (100) plane of γ-AlOOH only under relative high H^+ concentration. Herein, questions must be explained is what relative high H^+ is and what the differences among three models in experiments are. Three physical/chemical processes were involved in the reaction: protonation of surface hydroxyls, adsorption of H^+ on (100) plane and AlOOH dissolution process. Assuming that all the raw γ-AlOOH materials are *ca.* 5 nm nanoparticles, the molar amount of H^+ needed for surface protonation can be calculated according to the following equations. As shown in the equation (5), the total amount H^+ involves three parts: *(a)* $S*C$, for hydroxyls protonation, *(b)* $10^{-pH}V$, in solution, and *(c)* $S*\kappa_{100}\mu$, for formation of O-H bonds in (100) plane.

$$S = \frac{4\pi R^2 M}{\frac{4}{3}\pi R^3 \rho} = \frac{3M}{\rho R} \qquad (3)$$

$$\kappa_{100} = \frac{b*c}{a*b + a*c + b*c} \times 100\% \qquad (4)$$

$$n(H^{+}) = S*C + 10^{-pH}V + S*\kappa_{100}\mu \qquad (5)$$

Where S is the total surface area, M is the molar weight of AlOOH, ρ is the density of AlOOH, R is the radius of AlOOH particle, C is the surface concentration for hydroxyls, V is total volume of solution, κ_{100} is the area ratio of (100) plane calculated from bulk lattice, μ is number of exposed O atoms which can be protonated and $n(H^+)$ is the mole number of H^+ needed in theory.

The γ-AlOOH surface is considered to be fully protonated at low pH value (pH=1.7) and proton active surface concentration for hydroxyls is 1.7 sites per nm^2. Herein, the molar amount of H$^+$ needed in model a is only concerned with the first two items in eqn (5) in which only surface hydroxyls protonation process and H$^+$ in solution is considered. The calculated value is 0.014 mol, which is also the upper limit for obtaining pure γ-AlOOH phase. As for model b, according to the fully protonation model as shown in Figure S4, the value of μ is 4.3 per nm^2 and total molar amount of H$^+$ needed as discussed in model b is 0.102 mol which is also the lower limit for BAS phase appearance.

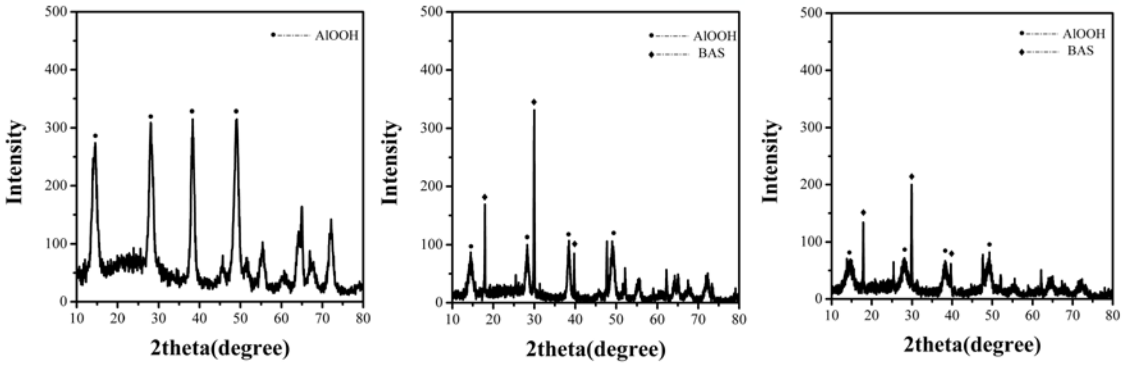

Figure 9. XRD pattern of product with molar amount of H$^+$, (a) 0.014 mol, (b) 0.102 mol (c) 0.080 mol.

To prove above conjecture, experiments, as in the typical synthesis, but with changes of theoretical molar amount of H$^+$ in model a and model b, were carried out. Indeed, pure γ-AlOOH phase and BAS phase were obtained in theoretical value as shown in Figure 9a and 9b, respectively.

However, it is found BAS phase can be obtained when the initial amount of H^+ is 0.080 mol which is a little smaller than the theoretical value and the deviation is ascribed to the size diversity of raw material comparing to the presumption and overestimate of the surface O atom density in (100) plane that can form O-H bonds (4.3 sites per nm^2 in theory).

Protonation process of surface hydroxyls in (010) and (001) planes is considered to be preferential to dissolution process in energy, because γ-AlOOH phase still exists as shown in Figure S7a when stoichiometric ratio of H^+ (0.133 mol) calculated according to eqn (1) and (2) was applied, which illustrated adsorption process was preferential and caused the shortage of H^+ in reaction. Herein, in the typical synthesis, the initial concentration of H^+ (0.160 mol) in the typical synthesis is identified as the optimal amount for preparing well-defined monodisperse microcrystals which is proved to be just sufficient for protonation and γ-AlOOH dissolution and excess amount of H^+ will cause second nucleation as shown in Figure S7b.

Generally, formation of a perfect crystal requires a slow and reversible pathway between the building blocks on the solid surface and those in a fluid phase, which allows the building blocks to easily adopt correct positions in developing the long range ordered crystalline.[30] In addition, the avoidance of second nucleation is necessary to obtain mono-disperse micro- and nanocrystals. Herein, limited by the dissolution rate of γ-AlOOH, building blocks on the BAS crystal surface have enough time to adjust their positions. Reaction mixture is still in suspending status instead of obtaining transparent solution and phase separation occurs after standing for 30 min at room temperature as shown in Figure S8, which illustrates the dissolution of γ-AlOOH into Al^{3+} is a relative slow reaction. Although hydrothermal treatment can accelerate the dissolution process, it still needs up to 30 min as prenucleation period for BAS formation which reveals dissolution of γ-AlOOH into Al^{3+} is the rate-controlling step and H^+ concentration is the critical factor for the formation of BAS phase. At the same time, the slow dissolution rate of γ-AlOOH and rapid growth of BAS leads to a low Al^{3+} concentration during the crystal growth and the second nucleation is successfully avoided, resulting in the monodisperse BAS crystals.

Herein, we mainly focus on the relationship between the molar amount of H^+ and final phase on the base of experimental results and DFT calculations. Influences of hydrothermal temperature on the phase and morphology were given in Figure S9. Furthermore, keeping other conditions unchanged, replacing 40 mmol H_2SO_4 with 40 mmol Na_2SO_4 results in the mixture of BAS and AlOOH. Combined with the effect of H^+ molar amount (Figure 9 and Figure S7), it can be concluded that rising temperature and increasing the H^+ amount can promote the formation of BAS by enhancing the dissolution of AlOOH, and SO_4^{2-} can promote the formation of BAS by affecting the chemical equilibrium of eqn (2). Summing up above analysis, formation of BAS is the result of a synergistic effect: (i) dissolution of γ-AlOOH, which is a slow process and the concentration of Al^{3+} is in an equilibrium state, (ii) formation of BAS, which depletes Al^{3+}, leading the equilibrium to shift towards right in equation (1). Moreover, H^+ created in equation (2) compensates part of that consumed, avoiding that the concentration of H^+ reduces too quickly.

Conclusions

In summary, a combination of experimental and computational approach was employed to gain insight into the possible formation mechanism of basic aluminium sulfate microcubes. From these results, basic aluminium sulfate microcubic crystals can be synthesized by facile hydrothermal process in large scale. Time dependent experiments illustrate the formation process of BAS controlled by two competing reactions follows the dissolution and recrystallization mechanism.

Meanwhile, dramatic structural changes occurred in (100) plane under high H^+ concentration which is inferred to be the initiation for source of Al^{3+}. Finally, exposed planes predicted surface energy calculation along with XRD pattern can well explain the formation of basic aluminium sulfate microcubes and its preponderant orients.

Supplementary Information

Electronic supplementary information (ESI) available. It contains XRD patterns of time-depended samples, crystal data for basic aluminium sulfate and electronic property of fully protonated (100) plane of γ-AlOOH.

Acknowledgments

This work is supported by the Major National Science and Technology Projects of China (2012ZX04007-021-04), the Key Projects in the Science & Technology Pillar Program of China (2011BAE33B01), and the Natural Science Foundation of Shandong Province (ZR2011BZ002).

References

1 A. P. Alivisatos, *Science*, 1996, **271**, 933-937.

2 (a) I. N. Bhattacharya, P. K. Gochhayat, P. S. Mukherjee, S. Paul and P. K. Mitra, *Mater. Chem. Phys.*, 2004, **88**, 32-40; (b) D. Donaldson, B. E. Raahauge, *Essential Readings in Light Metals*, W. C. Sleppy, A.Pearson, C. Misra and G. MacZura John, Wiley & Sons, Inc., 2013, pp 1111-1120.

3 G. Johansson, G. L. Lundgren, L. G. Sillén and R.Söderquist, *Acta Chem. Scand*, 1960, **3**, 769-771.

4 H. H. Willard and N. K. Tang, *J. Am. Chem. Soc.*, 1937**,** **59**, 1190-1196.

5 T. Sugimoto, H. Itoh and H. Miyake, *J. Colloid Interf. Sci.*,1997, **188**, 101-114.

6 L. V. Duong, B. J. Wood and J. T. Kloprogge, *Mater. Lett.*, 2005, **59**, 1932-1936.

7 T. He, L. Xiang and S. Zhu, *Langmuir*, 2008, **24**, 8284-8289.

8 L. A. Wijenayaka, G. Rubasinghege, J. Baltrusaitis and V. H. Grassian, *J. Phys. Chem. C*, 2012, **116**, 12566-12577.

9 (a) E. Laiti and L.-O. Öhman, *J. Colloid Interf. Sci.*, 1996, **183**, 441-452; (b) J. Nordin, P. Persson, E. Laiti and S. Sjöberg, *Langmuir*, 1997**, 13**, 4085-4093.

10 W. Kohn, A. D. Becke and R. G. Parr, *J. Phys. Chem.*, 1996, **100**, 12974-12980.

11 (a) R. Demichelis, Y. Noel, B. Civalleri, C. Roetti, M. Ferrero and R. Dovesi, *J. Phys. Chem. B*, 2007, **111**, 9337-9346; (b) M. Digne, P. Sautet, P. Raybaud, H. Toulhoat and E. Artacho, *J. Phys. Chem. B*, 2002, **106**, 5155-5162; (c) P. Raybaud, M. Digne, R. Iftimie, W. Wellens, P. Euzen and H. Toulhoat, *J. Catal.*, 2001, **201**, 236-246.

12 F. Mercuri, D. Costa and P. Marcus, *J. Phys. Chem. B*, 2009, **113**, 5228-5237.

13 X. Krokidis, P. Raybaud, A.-E. Gobichon, B. Rebours, P. Euzen and H. Toulhoat, *J. Phys. Chem. B*, 2001, **105**, 5121-5130.

14 A. Motta, M. P. Gaigeot and D. Costa, *J. Phys. Chem. C*, 2012, **116**, 12514-12524.

15 (a) Y. Liu, Z. Wang and Y. Suo, *J. Phys. Chem. C*, 2007, **111**, 3427-3432;(b) S. Abeysinghe, K. W. Corum, D. L. Neff, S. E. Mason and T. Z. Forbes, *Langmuir*, 2013, **29**, 14124-14134.

16 Y. Xia, L. Zhang, X. Jiao and D. Chen, *Phys. Chem. Chem. Phys.*, 2013, **15**, 18290-18299.

17 C. E. Corbato, T. R. Tettenhorst and G. G. Christoph, *Clays Clay Miner.*, 1985**, 33**, 71-75.

18 R. J. Hill, *Clays Clay Miner.*, 1981, **29**, 435-445.

19 M. D. Segall, J. D. L. Philip, M. J. Probert, C. J. Pickard, P. J. Hasnip, S. J. Clark and M. C. Payne, *J. Phys.: Condens. Matter*, 2002, **14** , 2717-2744.

20 D. M. Bylander and L. Kleinman, *Phys. Rev. B*, 1990, **41**, 7868-7871.

21 J. P. Perdew, K. Burke and M. Ernzerhof, *Phys. Rev. Lett.*, 1996, **77**, 3865-3868.

22 Y. Xia, X. Jiao, Y. Liu, D. Chen, L. Zhang and Z. Qin, *J. Phys. Chem. C*, 2013, **117**, 15279-15286.

23 (a) V. K. LaMer and R. H. Dinegar, *J. Am. Chem. Soc.*, 1950, **72**, 4847-4854; (b) H. Reiss, *J. Chem. Phys.*, 1951, **19**, 482-487.

24 Z. Li, L. Schulz, C. Ackley and N. Fenske, *J. Colloid Interf. Sci.*, 2010, **351**, 254-260

25 J. Nordin, P. Persson, E. Laiti and S. Sjöberg, *Langmuir*, 1997, **13**, 4085-4093.

26 M. A. Marques, M. A. S. Oliveira and J. R. Rodrigues, *J. Chem. Soc. Faraday Trans.*, 1990, **86**, 471-480.

27 J. Saukkoriipi and K. Laasonen, *J. Chem. Theory Comput.*, 2010, **6**, 993-1007.

28 Z. Berkovitch-Yellin, *J. Am. Chem. Soc.*, 1985, **107**, 8239-8253.

29 D. Du, D. J. Srolovitz, M. E. Coltrin and C. C. Mitchell, *Phys. Rev. Lett.*, 2005, **95**, 155503.

30 Y. Xia, P. Yang, Y. Sun, Y. Wu, B. Mayers, B. Gates, Y. Yin, F. Kim and H. Yan, *Adv. Mater.*, 2003, **15**, 353-389.